International Journal of Engineering Research in Africa
ISSN: 1663-4144, Vol. 39, pp 32-46
doi:10.4028/www.scientific.net/JERA.39.32

Submitted: 2018-02-20
Revised: 2018-09-07
Accepted: 2018-09-10
Online: 2018-11-05

Investigation of Temporary Overvoltage on Microgrid with Emphasis on Ferroresonance

Ajibola O. Akinrinde[a]*, Andrew Swanson[b] and Remy Tiako[c]

Discipline of Electrical, Electronic and Computer Engineering, University of KwaZulu-Natal Durban, South Africa

[a]tunjiakinrinde@yahoo.com, [b]Swanson@ukzn.ac.za, [c]Tiako@ukzn.ac.za

Keywords: Microgrid, Wind Energy, Photovoltaic System, Ferroresonance

Abstract. Temporary overvoltages caused by primary and secondary islanding due to a fault on a hybrid microgrid of a wind energy and PV system that was connected to the grid, was considered in this study. Symmetry opening of three poles opening and nuisance opening of circuit breaker leading to ferroresonance were investigated using ATP/EMTP. The findings show that during primary islanding an overvoltage of 5.60 P.U. was observed and 7.05 P.U. during secondary islanding. An overvoltage of 3.43 P.U. was experienced during an event of ferroresonance, which could be suppressed by transposing the cable and by connecting a resistive load which is 1% of rated transformer. The effect of the length of the cable on the ferroresonant overvoltage was also studied and found to decrease with the increase of the length of cable.

Introduction

Due to economical, technological, environmental and efficiency problems facing centralized power systems, these problems have paved the way for microgrid. A microgrid is a smaller version of a conventional grid, having the same structures as a conventional grid in terms of generation and distribution but eliminating the need for a transmission network so that the load and the power source are in close proximity. A microgrid is an integrated power system whose power generation could be from various power sources for the purpose of energy efficiency, environmental friendliness, sustainability, reliability and cost efficiency [1]. The power sources used are termed distributed generations (DGs) which are small size power sources supplied directly to the load, in order to improve contingencies in terms of cost, losses, efficiency and optimization attached to generation, transmission and distribution.

Distribution generations could either be conventional or nonconventional but the prime energy source behind the concept of microgrid is renewable energy. Penetration of renewable energy has gained great importance due to increase in demand for power, fear of depletion of conventional energy in the near future and concern towards global warming. Solar and wind energy are gaining attention among other renewable energy sources for microgrid purposes as their limiting factors such as initial cost of purchase, installation, power quality and storage are being significantly tackled.

A microgrid can operate as a standalone system in an island mode and can also be connected to the grid as a grid connected mode, this must be done according to IEEE 1547 standard [2] which gives guidelines and requirements for connecting a microgrid to the main grid. The microgrid could switch from the grid mode to island mode intentionally or unintentionally. In an event of fault occurring on the main grid, the isolating device should disconnect the microgrid from the grid, this is an unintentional scenario. In an event of maintenance of the grid, the microgrid can intentionally be disconnected from the grid either for maintenance or repair purposes. One of the dangers that could be associated with island mode operation of microgrid is temporary overvoltage which could be caused by switching operation or occurrence of fault. Events leading to temporary overvoltage include load rejection, fault clearance, short circuit fault, resonance and ferroresonance.

Ferroresonance is of great importance among other events in power systems and should be emphasized due to the increase in nonlinear components in power systems and its capability to cause severe overvoltage. Ferroresonance having a frequency range of 0.1 Hz – 1 kHz falls under low frequency transients, which may likely pose a threat to the life expectancy of the equipment. Ferroresonance is not as popular as resonance among existing literatures; however, considerable attention should be given to it because of the negative effects it could cause on the power systems. Such negative effects include; permanent overcurrent, permanent distortion of voltage and current wave forms, permanent overvoltage, displacement of neutral point voltage and overheating in transformers [3]. All these can lead to insulation breakdown and the eventual damage to the electrical devices on the power system. Ferroresonance occurs in an electric circuit containing non-linear inductance, capacitance, low losses and voltage source, hence it is necessary to investigate ferroresonance on microgrid since all these elements are present. Some researchers have worked on overvoltage as regards to microgrid; Vasquez-Arnez, et al. [4] worked on microgrid of PV system, wind power and hydroelectric and 1MW each by analyzing power frequency overvoltages rising from different types of faults ranging from line-to-ground to double line-to-ground during island mode. The result was compared to basic insulation level (BIL) of the system and the overvoltages were found not to be dangerous to the system as they were below BIL. However, their study was limited to fault analysis. Chen and Yu [5] did a review on overvoltage in a microgrid, discussing briefly ground fault overvoltage, resonant overvoltage, overvoltage as regards to voltage regulation and switching overvoltage of microgrid, and concluded that ferroresonance overvoltage and transfer overvoltage are the most severe compare to other overvoltages. Analysis of ferroresonance on microgrid of PV and wind system due to primary and secondary islanding was performed by George, et al. [6] using simulink as a tool of simulation. An induction generator was used as the wind turbine generator, while an inductor motor was used as a major load on the microgrid. The effects of compensating capacitor and different types of loads as regards the ferroresonance were studied. It was concluded that the absence of compensating capacitor in a microgrid could limit the occurrence of ferroresonance.

In this paper, a grid connected microgrid was investigated for temporary overvoltage during island operation of the microgrid using ATP/ EMTP. Ferroresonance resulting from primary isolation from the grid was analyzed as well as secondary isolation due to disconnection of the wind power system. The study further analyzed the effect of transposed cable, effect of cable length and effect of connected loads on the observed ferroresonance.

Modeling

The microgrid is made up of a wind turbine of doubly fed inductor generator (DFIG) and PV system connected to a weak grid as shown in Figure 1. The wind turbine generates voltage of 500 V which was stepped up to 11 kV and connected through an underground cable of 0.15 km long to the microgrid busbar. The output voltage of the PV system is 440 V. It was stepped up to 11 kV and finally connected to the microgrid busbar through 0.11 km long cable. An overhead transmission line with a length of 10 km connected the microgrid to the grid of 33 kV through a step-up transformer. In modeling the microgrid, ATP/EMTP software was used and the modeling was divided into three sections; modeling of PV system, wind turbine modeling and modeling of transformers.

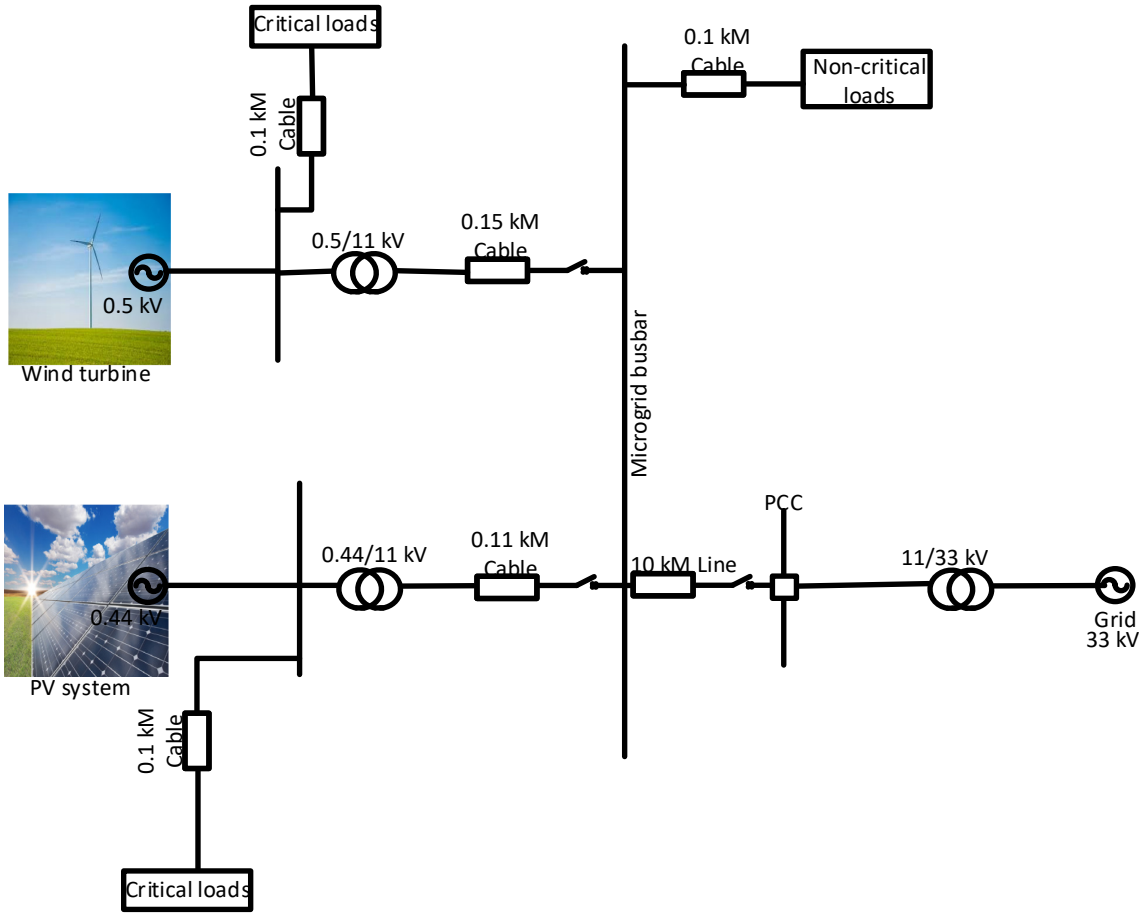

Figure 1: Microgrid architecture.

Modeling of PV System

The PV system comprised of arrays of solar panels which were arranged in series and parallel with each panel generating 150 watts. Aside from the solar cells, other PV system include boost converter, inverter, maximum power point tracking (MPPT) and other basic power equipment such as a transformer and filter. Solar cell is made up of semi-conductor material which allows current to flow through photovoltaic effect when light falls on it. Figure 2 shows a simple circuitry of a solar cell and Equation (1) and (2) show the currents flowing in a solar cell.

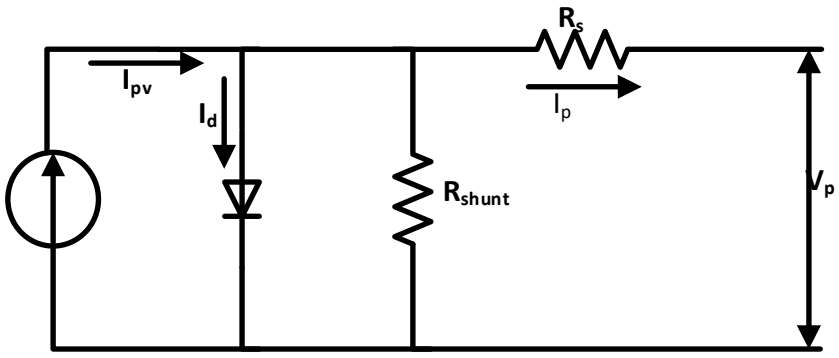

Figure 2: Simple circuitry of a solar cell.

I-V characteristics of an ideal solar cell is given as:

$$I_P = I_{pv} - I_d \quad (1)$$

$$I_d = I_o\left[\exp\left(\frac{q(V_p + R_s I)}{\propto kT} - 1\right) - \frac{V_p + R_s I}{R_{shunt}}\right] \quad (2)$$

Where, I_{pv} = current from the solar cell due to the photovoltaic effect, I_d = diode current, I_o = reverse saturation current , q = charge of the electron ($1.6x\ 10^{-19}$ c), α= diode quality constant, T = temperature of the solar cell, R_{shunt} = shunt resistance, R_s = series resistance, K = Boltzmann's constant ($1.3\ x\ 10^{-23}$ J/k), I = output current and V_p = output voltage.

The output voltage from the solar cells is boost by DC to DC converter and this is controlled by MPPT. The inverter is connected through the DC link converting the DC to AC. LCL filter cancel out destructive harmonics before it is supplied to critical loads and step up by the transformer to the grid.

Boost Converter

Figure 3 shows the schematic of boost converter. The boost converter increases the DC voltage obtained from the PV cells to higher voltage using the Equations (3) and (4);

$$\frac{dI_L}{dt} = \frac{1}{L}(V_p - V + V.S) \quad (3)$$

$$\frac{dV}{dt} = \frac{1}{c}(I_L - \frac{V}{R} - I_L.S) \quad (4)$$

$$S = \begin{cases} = 1 for\ on \\ = 0\ for\ off \end{cases} \quad (5)$$

Where I_L is the current across the inductor, V_p is the output voltage from the PV, V is the output voltage from the boost converter, S is the switching state of the IGBT.

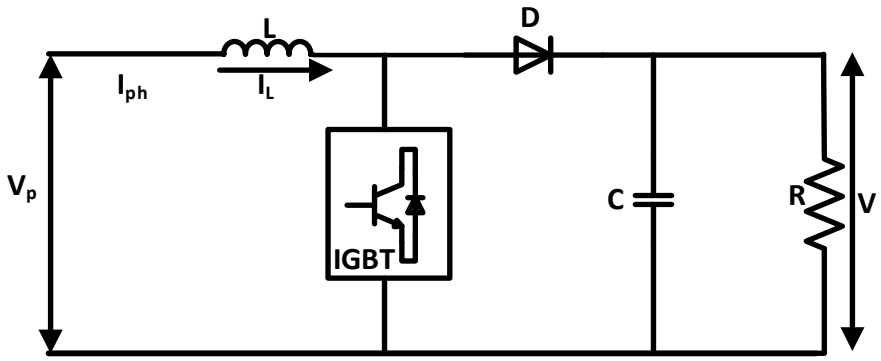

Figure 3: Schematic of boost converter.

MPPT

MPPT ensures that optimal power is delivered to the load. The power and voltage obtained from the PV cells is dependent on solar irradiance and temperature, under a certain condition of solar irradiance and temperature, the PV yields optimal power. There are several algorithms developed for MPPT of PV system, the scope of which is not considered in this research. However, the most popular algorithm is perturb and observe (P&O) algorithm, which is used in this study and presented in Figure 4.

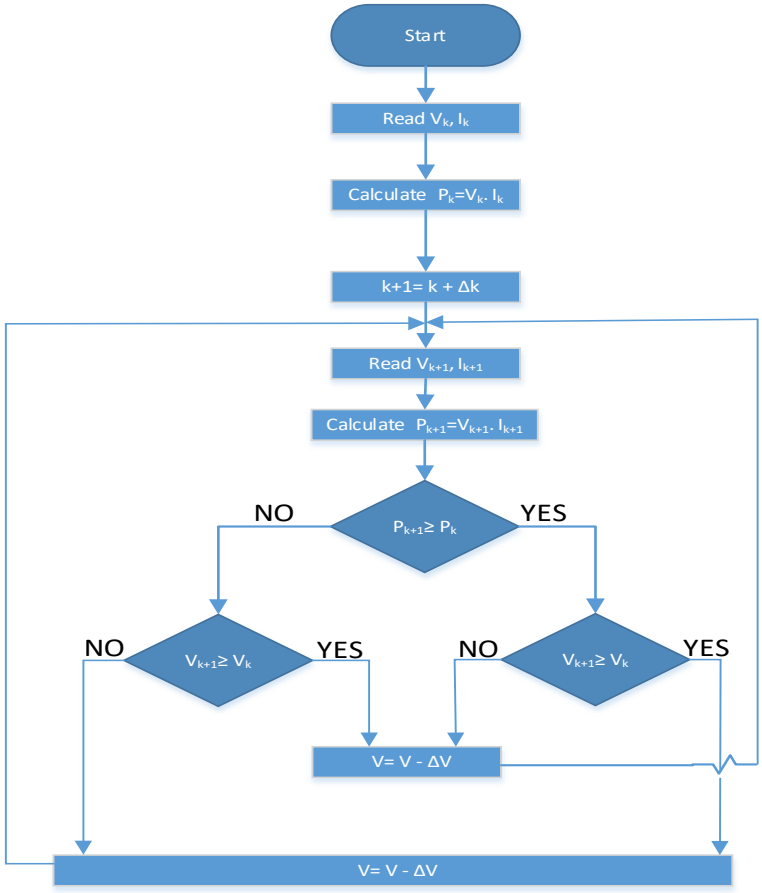

Figure 4: Flowchart of P&O algorithm.

Inverter and Control of PV Inverter

DC output of the boost converter is transformed to AC by the inverter which contains six electronics switching devices (IGBTs) which modulates the voltage according to the load. The control of the inverter is shown in Figure 5. Using Park transformation in Equation (6), the grid current and voltage are converted from A-B-C to d-q coordinate frame.

$$\begin{bmatrix} d \\ q \\ o \end{bmatrix} = \frac{2}{3}\begin{bmatrix} cos\theta & \cos(\theta - \frac{2\pi}{3}) & \cos(\theta + \frac{2\pi}{3}) \\ -sin\theta & -\sin(\theta - \frac{2\pi}{3}) & -\sin(\theta + \frac{2\pi}{3}) \\ \frac{1}{2} & \frac{1}{2} & \frac{1}{2} \end{bmatrix}\begin{bmatrix} A \\ B \\ C \end{bmatrix} \quad (6)$$

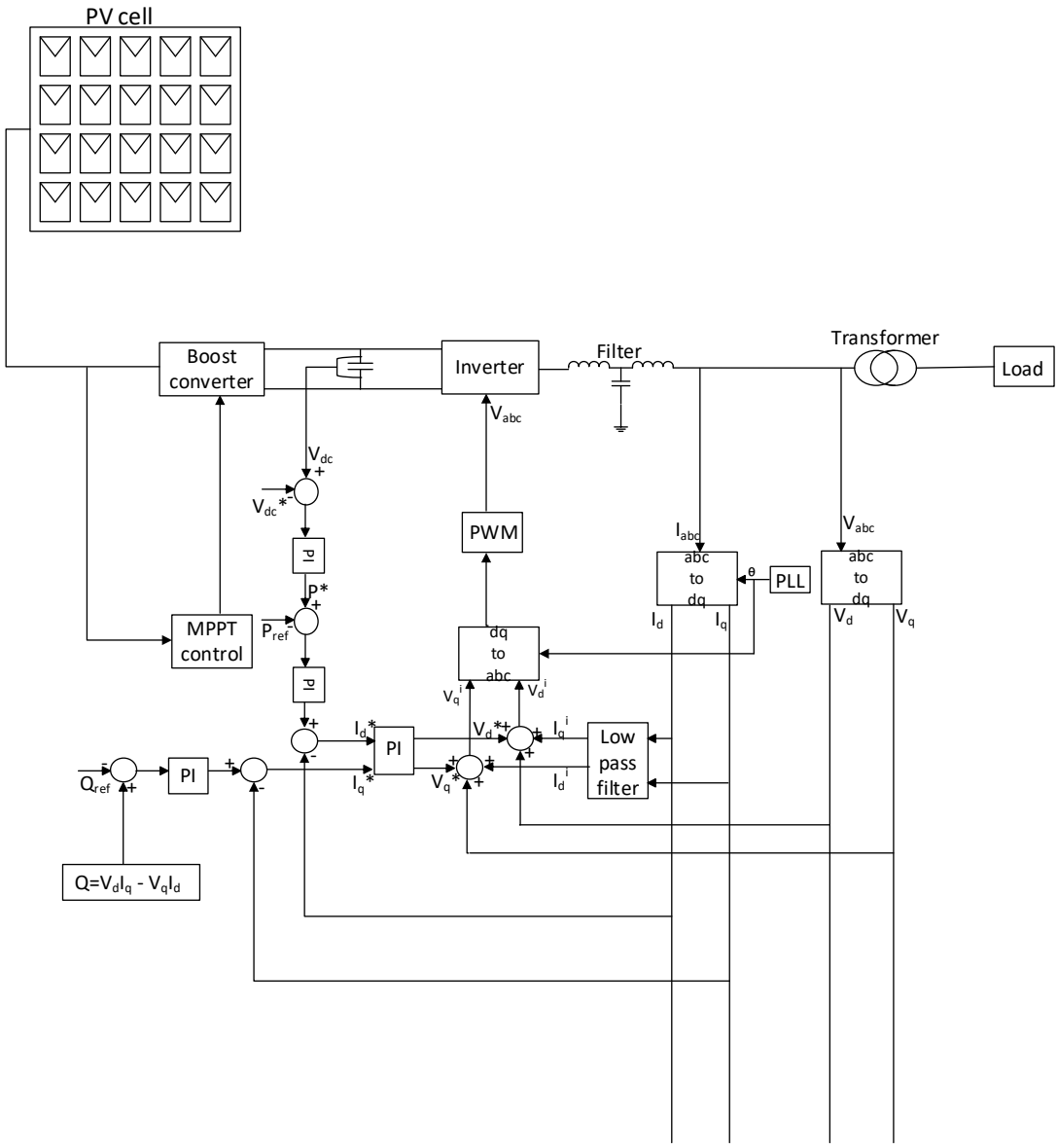

Figure 5: Control of PV inverter.

Wind Turbine Model

In modeling the wind turbine, DFIG wind turbine was considered because of its low cost, robustness and easy design and control. Variable-speed wind turbine is coupled with DFIG via gear box as shown in Figure 6, back-to-back converter is required immediately after the generator in order to reduce voltage disturbances from the generator. A capacitor was needed to compensate for the consumed reactive power, after which the wind turbine transformer steps up the voltage from 500 V to 11 kV.

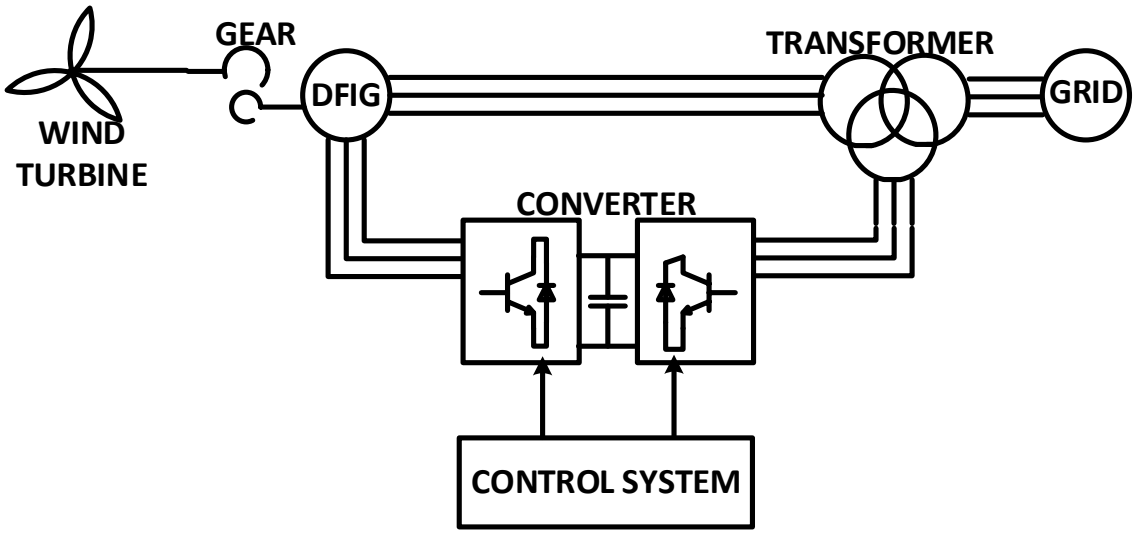

Figure 6: Schematic of DFIG wind turbine.

The aerodynamic power obtained from the rotation of the turbine blades is given as:

$$P_a = \frac{1}{2}A\rho v^3 C_p \tag{7}$$

Where A is the swept area, ρ is the density of the air, v is the speed of the wind and the C_p is the power coefficient of the turbine. The speed and torque of the generator are delivered by the gear box and can be obtained using Equation (8):

$$\frac{d}{dt}\omega_g = \frac{T_m - T_e}{J} \tag{8}$$

$$\omega_t = \omega_g K_{ratio} \tag{9}$$

Where, K_{ratio} is the gear ratio, J is the inertia constant, T_m and T_e are mechanical and electromagentic torque, ω_g and ω_t are the angular speed of the generator and turbine respectively.

Using machine model and assuming that the stator and the rotor windings are symmetrical and their quantities are arbitrary, the output voltages of the generator can be d-q sychronous reference frame as:

$$V_{sd} = R_s I_{sd} + \frac{d\varphi_{sd}}{dt} - \omega_e \varphi_{sq} \tag{10}$$

$$V_{sq} = R_s I_{sq} + \frac{d\varphi_{sq}}{dt} + \omega_e \varphi_{sd} \tag{11}$$

$$\varphi_{sd} = L_s I_{sd} + L_m I_{rd} \tag{12}$$

$$\varphi_{sq} = L_s I_{sq} + L_m I_{rq} \tag{13}$$

$$L_s = L_{is} + L_m \tag{14}$$

Where, L_s is the stator inductance, L_{is} is the stator self-inductance, L_m is the mutual inductance, I_{sd}, I_{sq} are the stator currents in d and q axis respectively I_{rd}, I_{rq} are the rotor currents in d and q axis respectively, φ_{sd}, φ_{sq} are the stator fluxes in d and q axis respectively and ω_e is the the synchronous angular speed.

The torque, active power and reactive power generated by the generator can be obtained using Equation (15), (16) and (17):

$$T_e = 1.5\, N_p \left(I_{sq}\varphi_{sd} - I_{sd}\,\varphi_{sq}\right) \quad (15)$$

$$P_s = 1.5 \left(V_{sq}I_{sq} + V_{sd}\,I_{sd}\right) \quad (16)$$

$$Q_s = 1.5 \left(V_{sq}I_{sd} - V_{sd}\,I_{sq}\right) \quad (17)$$

Where N_p is the number of the generator pole pairs.

Back-to-back converter consists of the stator side converter, dc linkage and grid side inverter as shown in Figure 7. Control of the converter cannot be undermined in obtaining desired voltage output; control of the stator side rectifier regulates the torque and the speed of the generator while control of the grid side inverter regulates the dc voltage, the active and reactive power. Control of both the stator side and the grid side converter is done using indirect field oriented control.

Control of Stator Side Converter

Stator side converter transforms the AC voltage from the wind generator to DC voltage. It is a full bridge rectifier consisting of six IGBTs. Control of a stator side converter is shown in Figure 7. The transformation of the rotor current and stator voltage from A-B-C to d-q coordinate frame using Equation (5). However, stator current is converted from A-B-C to α-β coordinate frame using Clarke transformation in Equation (18).

$$\begin{bmatrix} \propto \\ \beta \end{bmatrix} = \begin{bmatrix} 1 & \frac{-1}{2} & \frac{-1}{2} \\ 0 & \frac{\sqrt{3}}{2} & \frac{-\sqrt{3}}{2} \end{bmatrix} \begin{bmatrix} A \\ B \\ C \end{bmatrix} \quad (18)$$

Control of Grid Side Converter

The grid side converter is an inverter transforming the DC voltage from the rectifier to AC voltage. Control of the grid side converter is done by changing grid current and voltage from A-B-C to d-q coordinate frame using Equation (5) and it is decoupled. Figure 8 shows the regulation of the DC voltage by the DC link and passed through a PI controller. Desired reactive voltage Q_{req} is divided V_{gq} and regulated to obtain I_d^*. PI controller is applied to obtain V_d^* and V_q^* respectively. Phase locked loop (PLL) is used in order to synchronize the voltage and the frequency of the system to the grid. Finally, d-q coordinate frame is converted to A-B-C and PWM modulates the voltage.

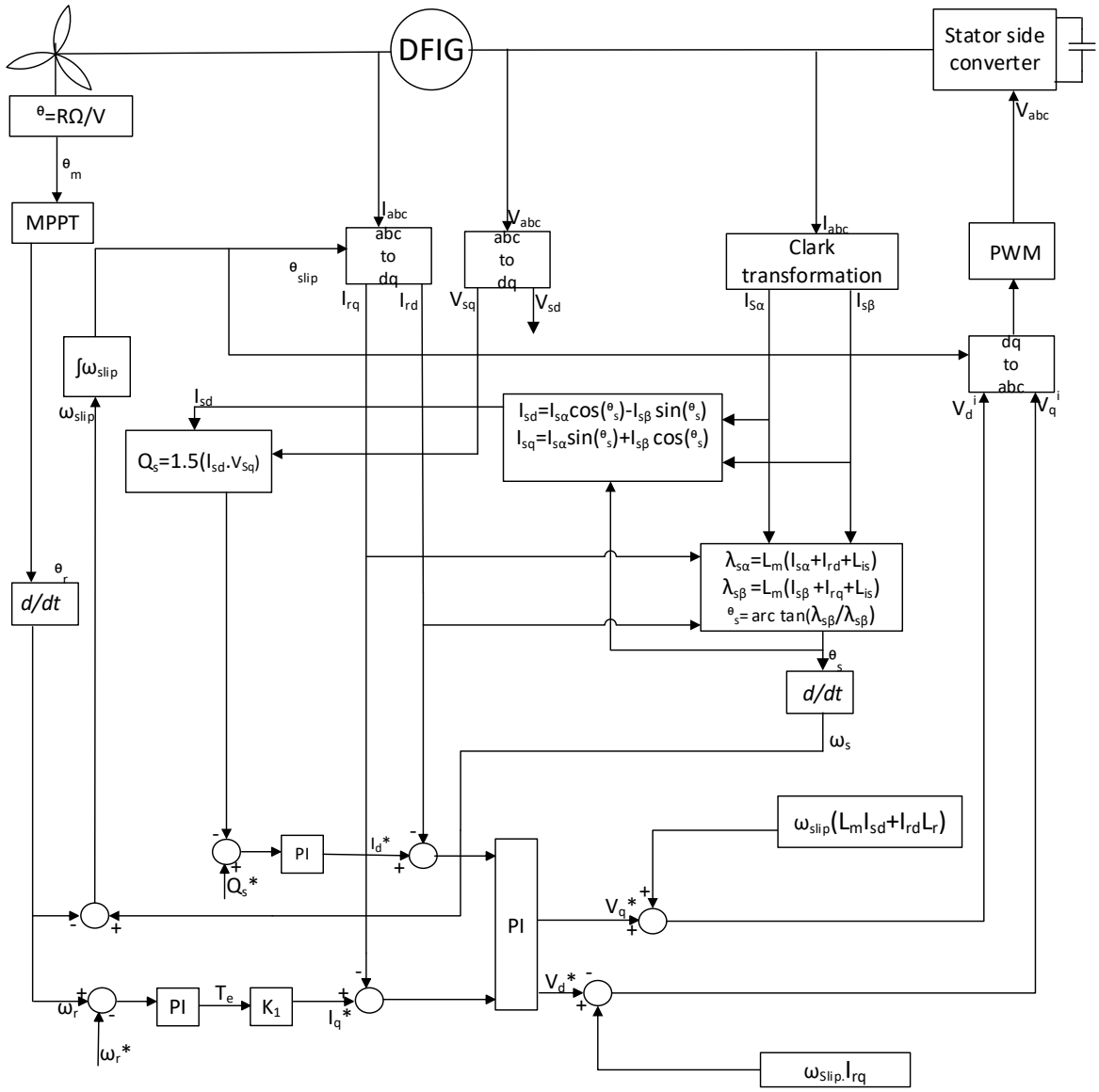

Figure 7: Control of stator side converter.

Where,

$$K_1 = \frac{L_s T_e}{N_p \varphi_{sd} L_m} \tag{19}$$

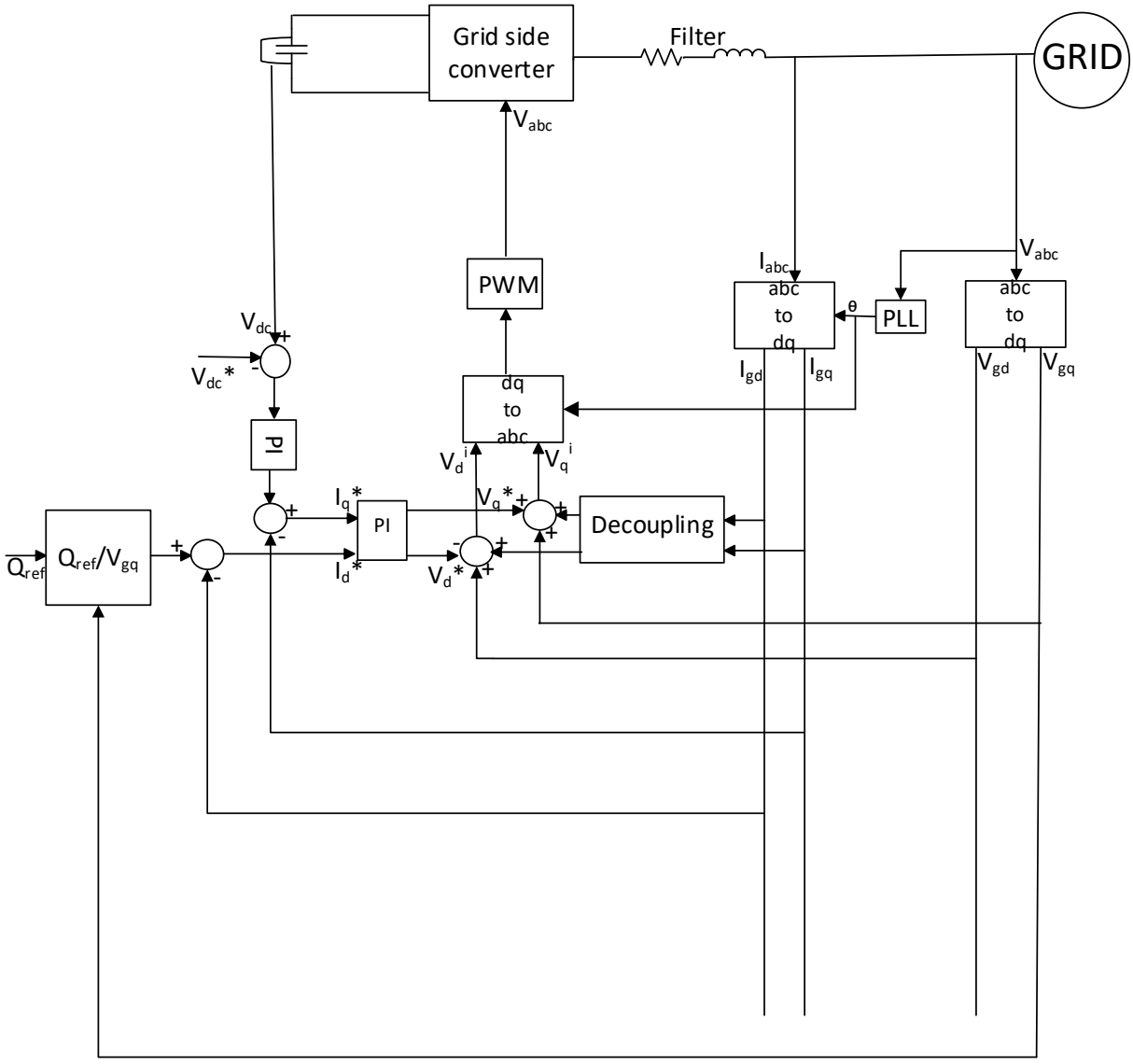

Figure 8: Control of grid side converter.

Transformers

All transformers in this model are represented using BCTRAN model available on ATP/EMTP. The wind turbine transformer and step-up transformer for PV are rated 1.5 MVA and 1 MVA respectively, while the transformer stepping to the grid is rated 6 MVA. The transformers are modeled according to low frequency transient classsification which considers modeling of nonlinearity as important especially the saturation characteristic of the core. Saturation characteristic of the core can be represented either by hysteretic or anhysteretic curve depicting the relationship between flux linkage and magnetizing current which can be calculated using a curve fitting function as show in Equation (20):

$$I = a\lambda + b\lambda^n \tag{20}$$

Where I is the magnetizing current, a and b are the constant coeffiecient for linear and saturated region respectively, λ is the flux linkage and n= 7..... and it is the number of degree order of the saturation.

Primary Islanding of the Microgrid

Grid connected microgrid could be islanded from the grid intentionally or unintentionally. Intentional islanding could be for the purpose of maintenance or repair on the grid and unitentional islanding could be as a result of fault or power quality issue as a result of discrepancy of power parmaters between grid and the microgrid, hence they are not synchronized, thereby forcing the circuit breaker at pcc to open. Islanding in microgrid is inevitable, therefore monitoring and control strategy measures are put in place to ensure the power stability during islanding, however, such control strategies are beyond the scope of this paper. Figure 9 shows the output voltage of grid connected microgrid, while Figure 10 depicts the voltage of the microgrid during primary islanding when it is disconnected from the grid at 0.8 secs. Overvoltage experienced as the circuit breaker opens is 5.60 P.U., which is higher than the permissive rated power frequency voltage level according to the IEC 60071-1 standard [7].

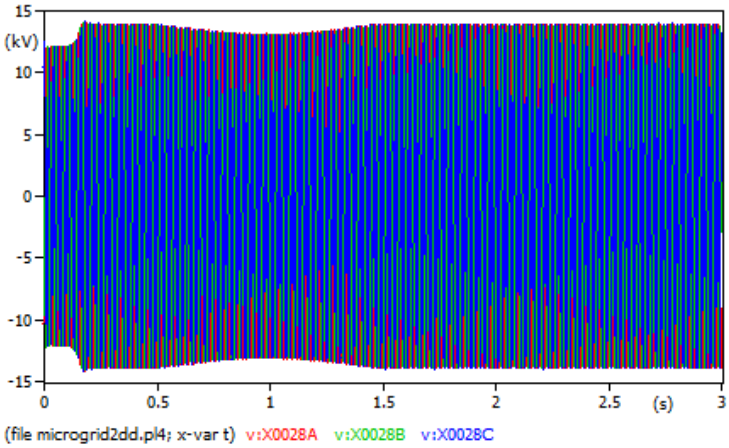

Figure 9: Output voltage of grid connected microgrid.

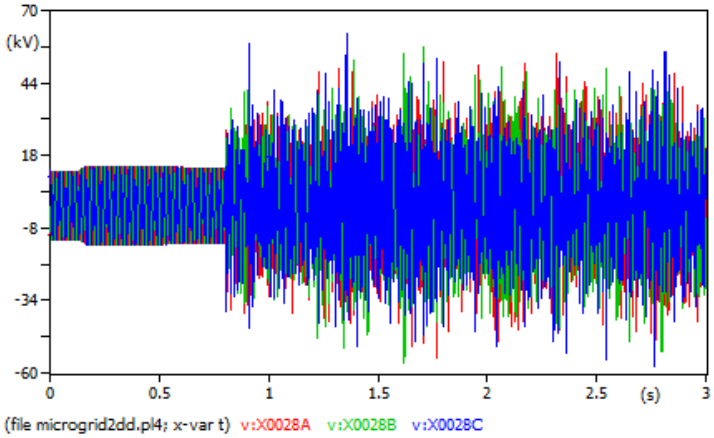

Figure 10: Primary islanding of the microgrid.

Secondary Islanding of the Microgrid

Secondary islanding could happen in a situation where the primary islanding had occurred and the steady performance of the microgrid is achieved, then all other DGs were disconnected such that only one DG is connected to the load. This situation could be catastrophic for the DG and its associated power equipment, thereby monitoring and control strategies to arrest secondary islanding in hybrid microgrid cannot be overemphasized. However, it is beyond the scope of this paper. In studying the occurrence of secondary islanding in this paper, the wind turbine was disconnected and two possible scenarios were investigated; three poles opening of the circuit breaker and two poles opening of the circuit breaker.

Three Poles Opening of the Circuit Breaker

Figure 11, shows proper opening of the circuit breaker the three poles of the breakers at 0.7 s, the overvoltage observed is 7.05 P.U, this is higher than the standard short duration power frequency voltage. The overvoltage is large at the time of opening and decays over the duration of 2.3 s to steady state. The extent of danger that the microgrid could experience due to proper opening of the breaker depends on the frequency of switching and how large is the transient and the sub-transient period during fault.

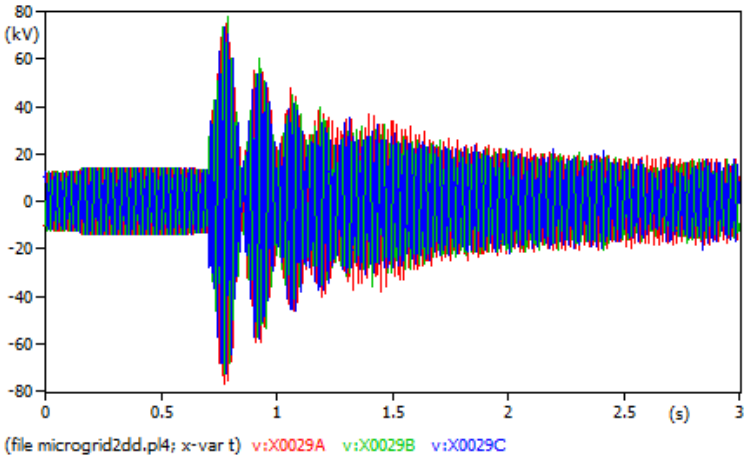

Figure 11: Three poles opening during secondary islanding of the microgrid.

Two Poles Opening of the Circuit Breaker

In this scenario, one of the poles of the circuit breaker was considered to be stuck, leaving two poles of the circuit breaker open due to nuisance operation of the breaker. This resulted in ferroresonance on the wind turbine, with an overvoltage of 3.43 P.U. shown in Figure 12, larger than the power frequency withstand voltage of the transformer. Even though the observed overvoltage during an event of ferroresonance was not as high during proper opening of the breaker, it is noted that the overvoltage during ferroresonance did not decay to steady state. The overvoltage existed for a longer time on the microgrid and this could have fatal effects over time on the power transformer; shortening their life span.

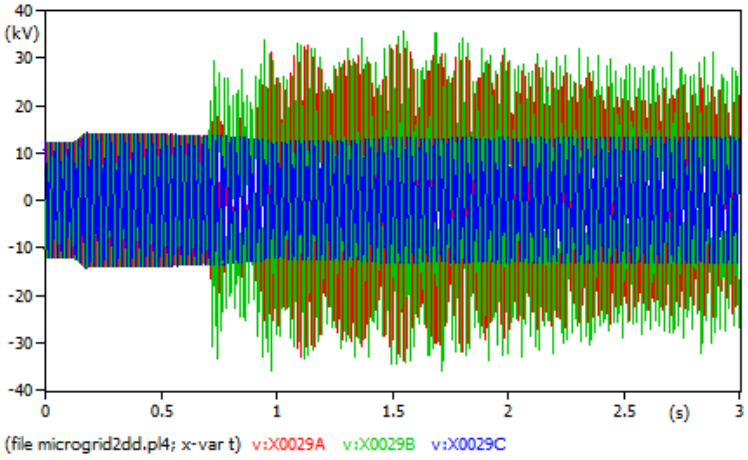

Figure 12: Two poles opening during secondary islanding of the microgrid.

Effect of Transposition of Cable on Ferroresonance Caused Nuisance Opening Operation of the Breaker

Transposition of the cable balance out the electrical elements of the three phase; Capacitance, inductance and resistance. The effect of transposition of cable supplying the non-critical load is investigated to observe its effect on the experienced overvoltage caused by ferroresonance. Figure 13 shows an overvoltage of 2.77 P.U. when transposed cable was used, however, the overvoltage is still greater than the rated power frequency voltage. Ferroresonance is caused by interaction of capacitance and saturable inductance during disturbance in the circuit, hence ferroresonance in this study is caused by the interaction of the capacitance of the cable and the transformer. Overvoltage of the transposed scenarios is less than an untransposed event because the capacitance on the three phase of the cable is balance. Unlike untransposed event, where capacitance on one of the phase would be higher and raise the overvoltage as it interacts with the transformer.

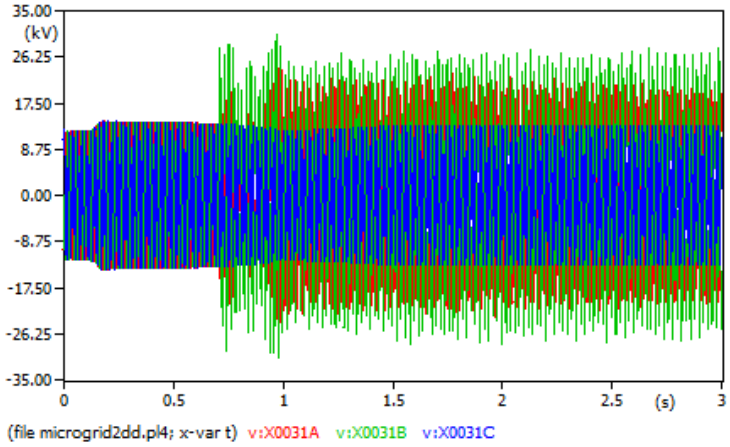

Figure 13: Effect of transposition of cable on Ferroresonance.

Effect of Length of Cable on Ferroresonance Caused by Nuisance Opening Operation of the Breaker

The effect of the length of cable supplying the non-critical load on the ferroresonance event recorded in Figure 12 was investigated. The cable was modelled using PI-model and the length of the cable connecting the wind turbine to the microgrid is 150 meters. However, the length of the cable ranged from 50 meters to 300 meters to investigate the effect of the cable length as shown in Figure 14. The overvoltage is found to be reducing as the length increased; this was due to the increase in the resistance of the cable hence, damping the overvoltage.

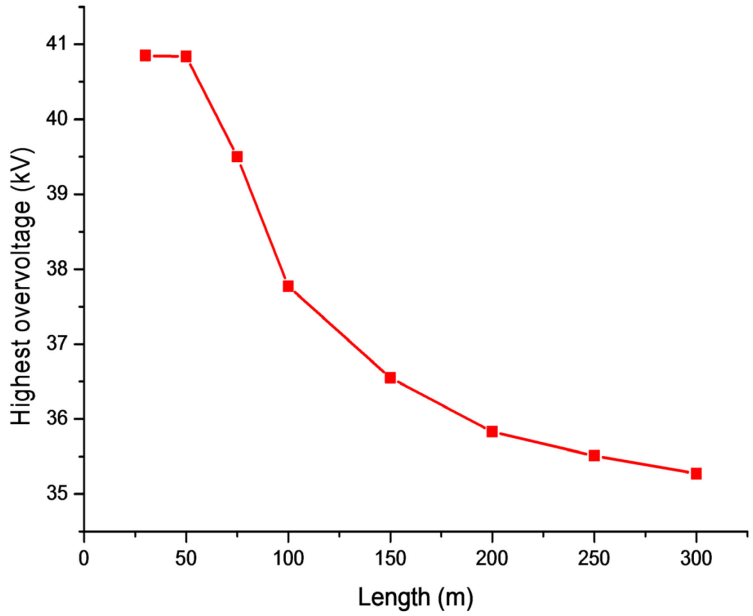

Figure 14: Effect of length of cable on ferroresonance.

Effect of Connected Resistive Load on Ferroresonance Caused by Nuisance Opening Operation of the Breaker

Connecting a load at the secondary side of the transformer is one of mitigation methods of suppressing ferroresonance. Theoretically, in order to avoid ferroresonance in power systems, a dummy load is attached at the secondary side of the transformer whose value is 5% that of transformer rating [8]. This value for the load is achieved by using Equation (21). However, the resistive load is varied from 500Ω to 5000Ω as shown in Figure 15. Resistive load at 5% of the rated transformer value, the overvoltage was found to be 1.81 P.U., however at 1%, overvoltage is found to be 1.23 P.U.

$$Restive\ Load = \frac{(Rated\ secondary\ voltage\ of\ the\ transformer\ )^2}{apparent\ power\ of\ the\ transformer} \tag{21}$$

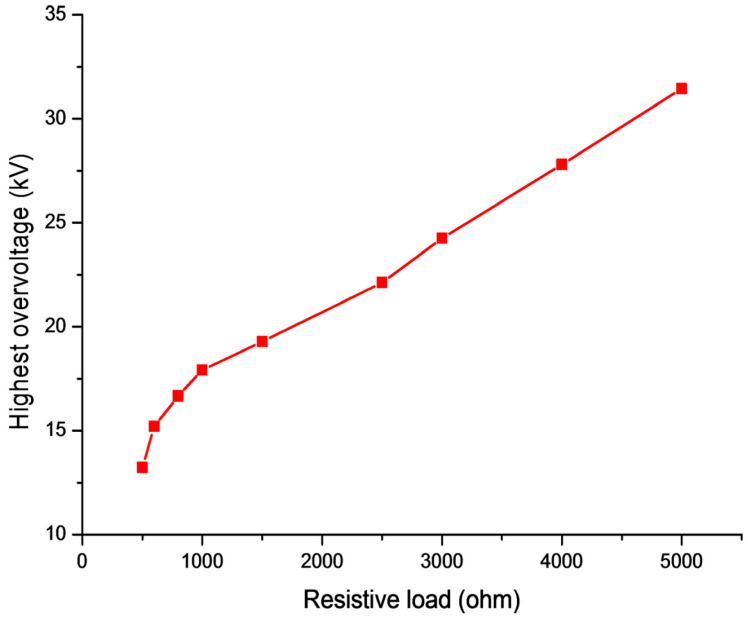

Figure 15: Effect of resistive load on ferroresonance.

Conclusion

Even though control strategies are implemented on microgrid, islanding of microgrid could still a pose danger to the microgrid over a period of time depending on the level P.U. of overvoltage and exposure period of the overvoltage. Simulation of islanding events was performed on hybrid microgrid of wind energy and PV system on ATP/EMTP and the results summarized as follows:

- During primary islanding of the hybrid microgrid from the grid, 5.60 P.U. overvoltage was experienced which did not decay over the 3seconds simulation time. The overvoltage is higher than the permissible power frequency voltage level and poses a danger to the life age of power equipment.
- 7.05 P.U. was observed during secondary islanding by opening the circuit breaker connecting the wind turbine to the microgrid. Overvoltage during secondary islanding was higher than the primary islanding event due to a rise in fault level as fault occurs closer to the source. This could cause harm to the generators.
- An event of ferroresonance was considered and 3.43 P.U. overvoltage was observed. Due to the undamp nature of the overvoltage, it poses a higher threat than three poles opening of the breaker. The transformer is in a danger of overheating as the overvoltage is higher than the rated withstand voltage.
- Transposition of the cable connecting the wind turbine microgrid was considered and the overvoltage reduces to 2.77 P.U. The effect of cable length on the overvoltage was also analyzed and found to decrease with increasing length of cable. Finally, the ferroresonance was mitigated by connecting a load whose value is 1% of the power transformer rating.

Reference

[1] A. Ali, W. Li, R. Hussain, X. He, B. W. Williams, and A. H. Memon, "Overview of Current Microgrid Policies, Incentives and Barriers in the European Union, United States and China," *Sustainability,* vol. 9, p. 1146, 2017.

[2] T. S. Basso and R. DeBlasio, "IEEE 1547 series of standards: interconnection issues," *IEEE Transactions on Power Electronics,* vol. 19, pp. 1159-1162, 2004.

[3] P. Ferracci, "<Additional Reference Schneider Electric CT 190 Ferroresonance.pdf>," in *Cahiers Techniques*, S. Electric, Ed., ed, 1998.

[4] R. L. Vasquez-Arnez, D. S. Ramos, and T. E. D. C. Huayllas, "Overvoltage Condition Assessment of a Microgrid Due to Faults Occurring in the Islanded Mode of Operation," *Energy and Power Engineering,* vol. 07, pp. 525-534, 2015.

[5] S. Chen and H. Yu, "A review on overvoltages in microgrid," in *Power and Energy Engineering Conference (APPEEC), 2010 Asia-Pacific*, 2010, pp. 1-4.

[6] V. George, G. K. Kumaran, J. Shivashankari, and S. Ashok, "Analysis of ferroresonance in a hybrid micro-grid with multiple distributed resources," in *Electrical, Electronics, and Optimization Techniques (ICEEOT), International Conference on*, 2016, pp. 1286-1291.

[7] IEC, "60071-1," in *Insulation Co-ordination-Part* vol. 1, ed, 2006, p. 67.

[8] J. Horak, "A review of ferroresonance," in *Protective Relay Engineers, 2004 57th Annual Conference for Protective Relay Engineers*, 2004, pp. 1-29.